Entropy **2015**, *17*, 4809-4837; doi:10.3390/e17074809

OPEN ACCESS

entropy

ISSN 1099-4300

www.mdpi.com/journal/entropy

Article

Power-Type Functions of Prediction Error of Sea Level Time Series

Ming Li [1] *, Yuanchun Li [2] and Jianxing Leng [1]

[1] Ocean College, Zhejiang University, Hangzhou 310058, China; E-Mail: jxleng@zju.edu.cn

[2] School of Information Science and Technology, East China Normal University, Shanghai 200241, China; E-Mail: liyuanchun510@hotmail.com

* Author to whom correspondence should be addressed; E-Mail: ming_lihk@yahoo.com.

Academic Editor: Carlo Cattani

Received: 27 April 2015 / Accepted: 3 July 2015 / Published: 9 July 2015

Abstract: This paper gives the quantitative relationship between prediction error and given past sample size in our research of sea level time series. The present result exhibits that the prediction error of sea level time series in terms of given past sample size follows decayed power functions, providing a quantitative guideline for the quality control of sea level prediction.

Keywords: sea level time series; prediction error; long-range dependence; power law

1. Introduction

Time series prediction gains interests of people in various fields of sciences and engineering, see for example [1–20], simply mentioning a few. Prediction of sea level time series (sea level for short) is desired in geosciences and ocean engineering [21–23], for many purposes such as understanding fluctuations of sea level rise, its dynamics and so forth [24–31]. Various methods and technologies have been reported for time series prediction, such as linear predictors [32–41], nonlinear predictions [42–46], and those based on artificial intelligence, including fuzzy systems [47–51] and artificial neural networks (ANN) [52–70].

This paper presents our study in the aspect of sea level time series prediction using the real sea-level data recorded by the National Data Buoy Center (NDBC) at the time scale of hour. The data are publicly accessible via http://www.ndbc.noaa.gov/historical_data.shtml. The predictor we utilized in this

research is an ANN predictor of the back propagation (BP) type, which is available in the toolbox of the software Matlab. Two highlights of this paper are as follows.

- We established the quantitative relationship between the past sample size, used for the predicting 40 points ahead of sea level time series as a case, and the prediction error characterized in the form of mean square at measurement stations of sea level time series we investigated.
- We obtained the analytic expression of that relationship in the form of power function, providing a guideline for the quality control in sea level prediction.

The rest of the paper is organized as follows. The research background, including the problem statement, is explained in Section 2. The research method is discussed in Section 3. Results are given in Section 4, which is followed by conclusions.

2. Research Background

2.1. Data

NDBC is an abbreviation, standing for a part of the US National Weather Service (NWS). It provides data for academic research, including sea level (see http://www.ndbc.noaa.gov/historical_data.shtml). We use the data recorded at the stations named LKWF1, SMKF1, LONF1, SAUF1, SPGF1, and VENF1, respectively. In terms of the names of the measurement stations, LKWF1 implies the station at Lake Worth, FL, USA (http://www.ndbc.noaa.gov/station_page.php?station=LKWF1); SMKF1 is the station at Sombrero Key, FL, USA (http://www.ndbc.noaa.gov/station_page.php?station=SMKF1); the station LONF1 is the one at Long Key, FL, USA (http://www.ndbc.noaa.gov/station_page.php?station=LONF1); the station SAUF1 is at St. Augustine, FL, USA (http://www.ndbc.noaa.gov/station_page.php?station=SAUF1); SPGF1 is at Settlement Point, GBI, Bahamas (http://www.ndbc.noaa.gov/station_page.php?station=SPGF1); and VENF1 is at Venice, FL, USA (http://www.ndbc.noaa.gov/station_page.php?station=VENF1). They are located in Florida, on the east coast of the Gulf of Mexico. The data are under the directory of Water Level, which is publicly accessible (http://www.ndbc.noaa.gov/historical_data.shtml#wlevel), referring Gilhousen [71] as an instance of research using the data by NDBC.

Six real traces of sea level time series described in Table 1 are selected in our research, where x_lkwf1_1999(t) denoted the sea level time series in 1999 at the station LKWF1, x_ven1_2003(t) the sea level time series in 2003 at the station VENF1, and so forth. Our selection of the above data is quite arbitrary in this research, simply for the purpose of study of prediction error of sea level without any conflict of interests regarding other manuscripts.

Table 1. Measured data of six traces of sea level time series.

Series Name	Record Date and Time	Data Size	Measurement Station
x_lkwf1_1999(t)	0:00, 1 Jan.–23:00, 31 Dec. 1999	8760	LKWF1
x_smkf1_2003(t)	0:00, 1 Jan.–23:00, 31 Dec. 2003	5851	SMKF1
x_lonf1_2003(t)	0:00, 1 Jan.–23:00, 31 Dec. 2003	8697	LONF1
x_sauf1_2001(t)	0:00, 1 Jan.–21:00, 31 Dec. 2001	8758	SAUF1
x_spgf1_1996(t)	0:00, 1 Jan.–23:00, 15 Dec. 1996	8616	SPGF1
x_ven1_2003(t)	0:00, 1 Jan.–23:00, 31 Dec. 2003	8760	VENF1

2.2. Problem Statement

Let $n > 0$ be the past sample size. Denote by $m \geq 0$ the step number of prediction. Then, random variables $x(i)$s for $i < n$ are the past records. Rewrite the n past records by $x(i-1), x(i-2), \ldots, x(i-n)$. Following Kolmogorov [72], with the selection of proper real coefficient a_s, one may obtain the linear combination of the n past records expressed by

$$L = \sum_{s=1}^{n} a_s x(i-s). \tag{1}$$

The above L may be used to predict a future value expressed by $x(i+m)$. Denote by e^2 the mean square error (MSE) given by

$$e^2 \triangleq e^2(n,m) = \mathrm{E}[x(i+m) - L)]^2, \tag{2}$$

where E is the mean operator. Kolmogorov stated that the $e^2(n, m)$ does not increase as n increase (Kolmogorov [72]), which yields a consequence we express as Corollary 1.

Corollary 1. *For a given m, the following holds*

$$e^2(n_2, m) \leq e^2(n_1, m) \text{ if } n_2 > n_1. \tag{3}$$

Note that the above is a general expression in quality with respect to $e^2(n, m)$. For a given time series $x(i)$, however, it does not tell us, quantitatively, how large $e^2(n, m)$ is with the past sample size n and the $x(m)$ to be predicted. For that reason, we consider the solution to the problem described below, aiming at establishing a quantitative relationship between the past sample size n and the given error provided that the step number of prediction m is predetermined.

Problem 1. *Let x(i) be a sea level time series. For a fixed m and given error* e_1*, what is the past sample size, denoted by* N_1*, required such that*

$$e^2(n,m)\big|_{n=N_1} = e^2(N_1,m) = e_1^2 \,? \tag{4}$$

Note 1. *The solution to the above problem is to find the function denoted by* $e_1(N_1, m)$*. An alternative solution is* $N_1(e_1, m)$*, which is in fact the inverse of* $e_1(N_1, m)$ *with respect to* N_1*.* □

2.3. Research Thoughts

We divide the task mentioned in Note 1 into two subtasks as follows.

- First, we find the $e_1(n, m)$ expressed only by an empirical curve based on processing real data of sea level.
- Then, by fitting the data, we may find the analytic expression of $e_1(n, m)$ as well as $e_1(N_1, m)$.

2.4. BP-ANN Predictor

Artificial neural networks (ANNs) are computational non-linear models that mimic the structures and functions of animals' nervous systems. ANNs, composed of interconnected neurons, are used to "learn" the complex relationship between input data and output data. Back propagation (BP) neural networks, one of the most important models in ANNs [73], are widely used in the fields of economy, ecology, meteorology, hydrology, medicine, *etc.*, see, for example, [74–77].

A BP neural network (BPNN), composed of one input layer, one or more middle layers called hidden layers and one output layer, can be seen as a non-linear input-output map, in which any two of these adjacent layers are interconnected directly while neutrons in each layer are independent.

As previously mentioned, the current value of a time series is based on the previous observed values. In this paper, every 21st sample is obtained by its previously successive 20 samples. Thus, the three-layer BP neural network is comprised of 20 inputs and 1 output (see Section 4.5). The n samples are divided into two sets to train and test the neural network predictor. Specifically, the first (n = 20) groups of samples are training data and the last 20 data are used to test the predictor. Every time the sample size changes, the number of samples for training is changed, while the numbers of neurons in input and output layers are constant. For example, if the sample size is 200, the inputs of the BPNN predictor are 20-dimensional vectors, containing the samples from the 1st to the 20th, from the 2nd to the 21st, and so forth, up to the last vector which contains the testing samples from the 180th to the 199th to train the network. Output data are the 21st to the 200th of the one-dimensional original data, corresponding to the 180 vectors in the input layer. For the testing sample, the 201st value can be obtained from its former data, referring to the samples from the 181st to the 200th. The 202nd value is the output of the predictor, whose inputs are the data from the 182nd to the 200th and the 201st value, which is a predicted value. The rest predicted values can be generated by this means. In this paper, annual data from the 5001st to the 5040th recorded by each station are predicted. The predicting process is shown in Figure 1.

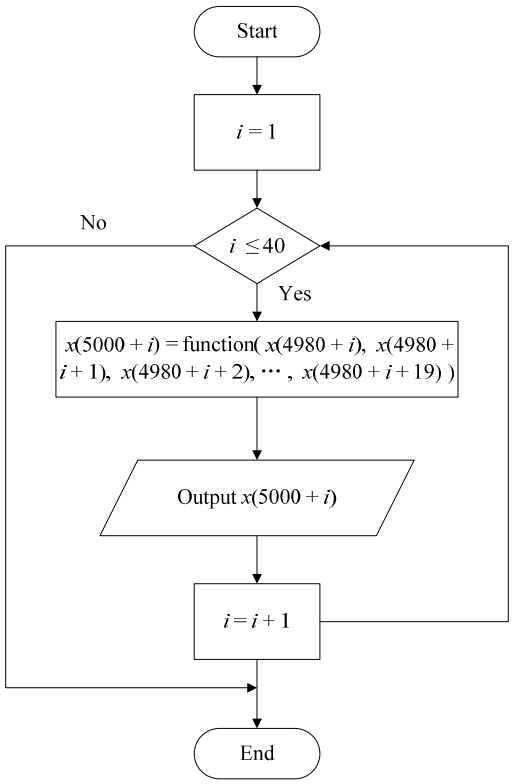

Figure 1. Process of predicting sea level time series from the 5001st value to the 5040th value.

Once the sizes of input and output layer are fixed, the optimal number of hidden layer and the number of nodes in hidden layer becomes a major challenge, see, for example, [78,79]. Any continuous and bounded real-valued function, based on Kolmogorov theorem [72,80], can be expressed as a three-layer

back propagation neural network, in which there are $(2k + 1)$ nodes for the middle layer, where k is the number of the input nodes. Thus, in this paper, one single hidden layer with 41 nodes is used for the BPNN model.

The transfer function, called activation function, represents the relationship between input and output of each node. Activation functions are required to be monotonic increasing and differentiable [81]. Sigmoid function, as a continuous and bounded function, is commonly used in input and hidden layers [82,83], which is expressed by

$$f(u) = \frac{1}{1 + e^{-u}}, \tag{5}$$

where u stands for the input of a single neuron. For the input layer, u is the input vector, which is the normalized sea level time series $x(t)$, while for the hidden layer, u is the weighted sum of outputs of the previous layer subtract the threshold value of the layer. Linear transfer function is used for the neurons in output layer, so that the outputs of the entire network can take any values.

BP neural networks are trained by adjusting the weights between two layers and threshold values based on the gradient steepest descent method, that is, if the errors between actual outputs and expected ones are not satisfied, the errors will propagated backward to adjust weights and threshold values repeatedly until the performance of the system such as mean square error (MSE) is minimized.

The available data are always divided into two sets, namely training and testing datasets. In order to obtain precise results and to reduce running time, it is necessary to normalize the available datasets to a range between zero and one [84], before training process with the formula below:

$$\overline{x} = \frac{x - x_{\min}}{x_{\max} - x_{\min}}, \tag{6}$$

where $x_{\max}$ and $x_{\min}$ are, respectively, the maximum and minimum values of the sample data $x(t)$. The final forecasting results are obtained by the following inverse normalized formula:

$$x = \overline{x}(x_{\max} - x_{\min}) + x_{\min}. \tag{7}$$

3. Experimental Methods

In this research, Neural Network (NN) Toolbox of the software MATLAB R2012b is used to realize the neural network predicting model. MATLAB is a multi-paradigm environment for numerical computing developed by MathWorks, Natick, USA. NN Toolbox, based on neural network theory, provides functions to design, train, visualize and simulate all kinds of networks such as linear network, BPNN, radial basis function NN, regression NN and so on [85,86]. Three functions: newff, train and sim are used in the learning procedure in the MATLAB commands [87].

As previously mentioned, the original dataset is divided into training and testing sets. In order to reduce prediction error, the data values are normalized between 0 and 1 via the function mapminmax. Function newff, which is used to generate and initialize a BP neural network, defines sizes and activation function of every layer and type of training algorithm. In this research, we use the function logsig between the input and hidden layers. The outputs of logsig are limited over the interval from 0 to 1 while its inputs can be taken with any value from negative infinity to positive infinity [88,89]. The transfer function purelin is used between the hidden and output layers so that the outputs of the network could

be arbitrary values. After creating a BP neural network, functions train and sim are used to train and simulate the net.

Without loss of generality, data used as samples are recorded at the six aforementioned stations, a total of approximately 8700 values annually in every experiment. For each station, the first set of samples is sea level from the 4901st to the 5000th of the original data, 100 values in total. In this paper, the step number of prediction is 40, that is, values from the 5001st to 5040th are predicted. Compared with the actual data, we can get the mean squared prediction error from the Equation (2). The second set of sample data are from the 4801st to the 5000th, 200 data totally. Then original data from the 4701st to the 5000th are chosen as the third set and so on, until the 15th set of sea level data from the 3501th to the 5000th. Fiften mean square errors, which are 15 points generated by 15 sets of samples, constitute a curve envelope, which can be fitted by specific functions. In this way, we can get the quantitative relationship between sample size and prediction error.

4. Results

4.1. Prediction Results

We selected the data recorded at the station LKWF1 in 1999 for demonstration. The original sea level series contains 8641 points of data, some of these are shown in Figure 2. When we used the past sample records of 100 data points from the 4901st point to the 5000th to predict the next 40 data points, the prediction error, MSE, is 0.38664. The original data of 40 points and their predictions are indicated in Figure 3. Figure 4 shows the prediction results when the past sample size is increased to be 200, that is, the past sample records contain the data from the 4801st point to the 5000th, to predict the next 40 data points. By eye, one may see that the prediction error in Figure 4 is smaller than that in Figure 3. When increasing the past sample size to 300, which includes the data from the 4701st point to the 5000th, to predict the next 40 data points, we obtained the results shown in Figure 5, which clearly exhibits that the prediction error in this case is smaller than that described in Figure 4. In Figures 6–17, the demonstrated prediction results based on the past sample records are from 400 to 1500; that is, using the past sample records from the 4601st–3401st point up to the 5000th, to predict the next 40 data points. Those figures again exhibit that the prediction error is decreased as the past sample size increases, which is consistent with the description of Kolmogorov in [72].

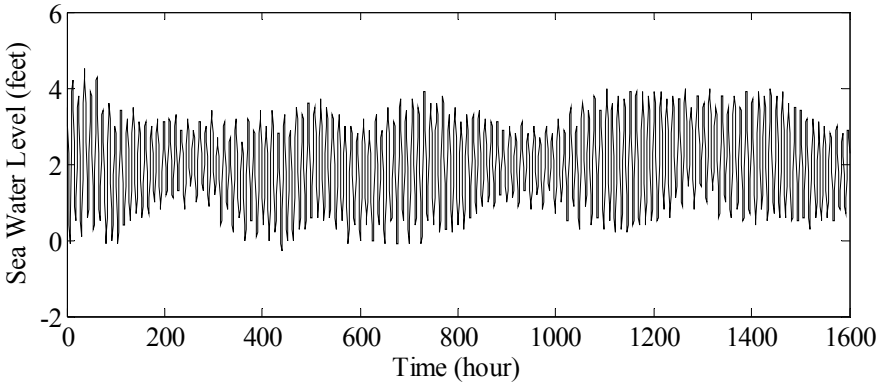

Figure 2. Sea level series at the Station LKWF1 in 1999.

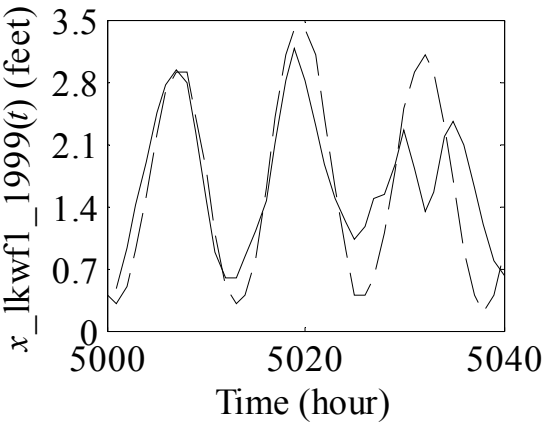

Figure 3. Prediction results with the sample size 100 at the Station LKWF1 in 1999. Solid line: predicted values, dashed line: original values.

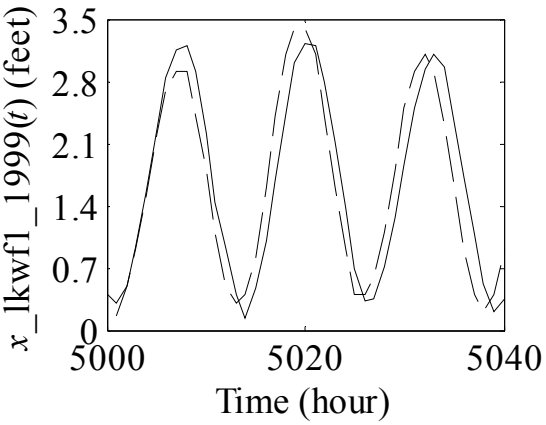

Figure 4. Prediction results with the sample size 200 at the Station LKWF1in 1999. Solid line: predicted values, dashed line: original values.

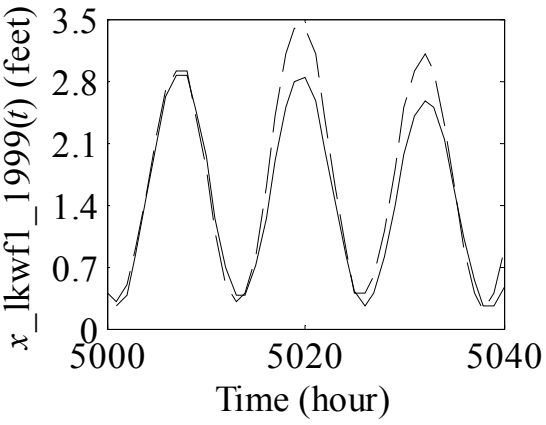

Figure 5. Prediction results with the sample size 300 at the Station LKWF1 in 1999. Solid line: predicted values, dashed line: original values.

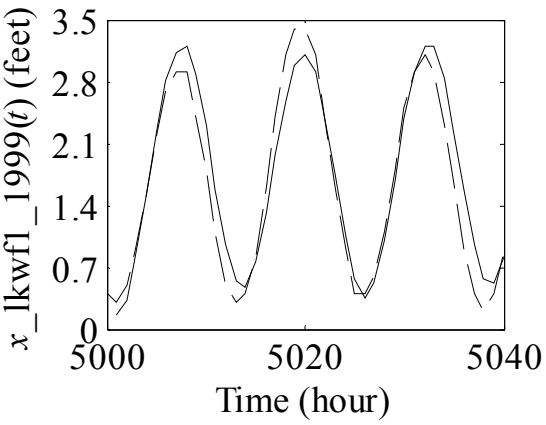

Figure 6. Prediction results with the sample size 400 at the Station LKWF1 in 1999. Solid line: predicted values, dashed line: original values.

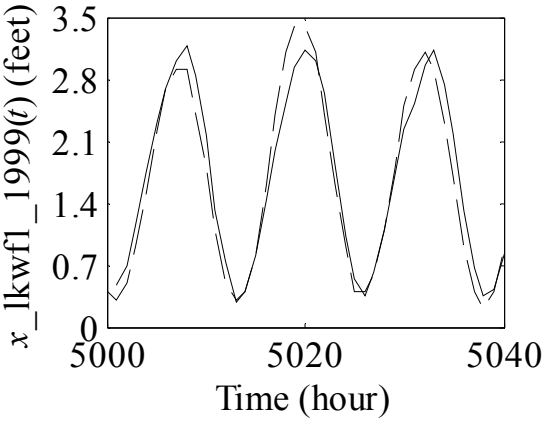

Figure 7. Prediction results with the sample size 500 at the Station LKWF1 in 1999. Solid line: predicted values, dashed line: original values.

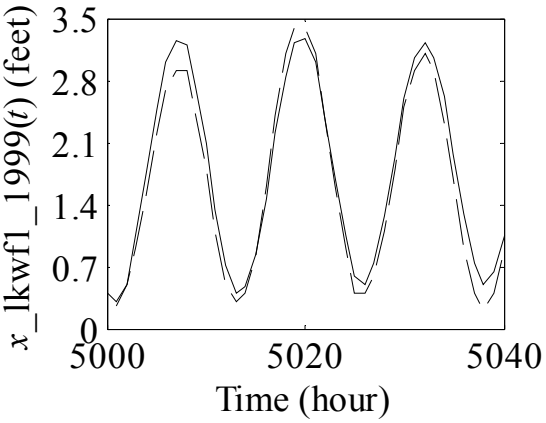

Figure 8. Prediction results with the sample size 600 at the Station LKWF1 in 1999. Solid line: predicted values, dashed line: original values.

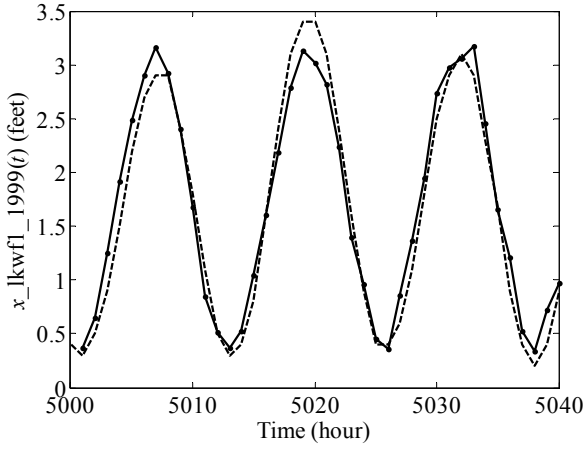

Figure 9. Prediction results with the sample size 700 at the Station LKWF1 in 1999. Solid line: predicted values, dashed line: original values.

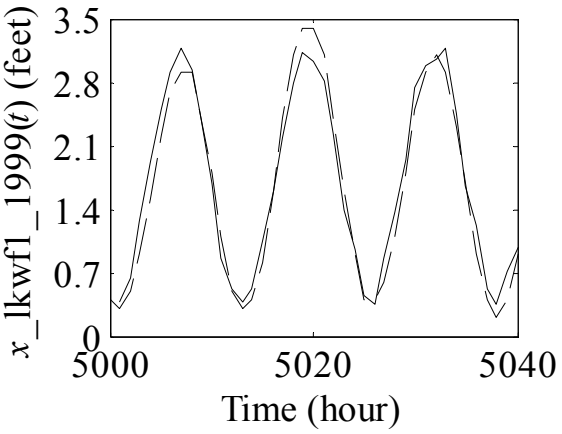

Figure 10. Prediction results with the sample size 800 at the Station LKWF1 in 1999. Solid line: predicted values, dashed line: original values.

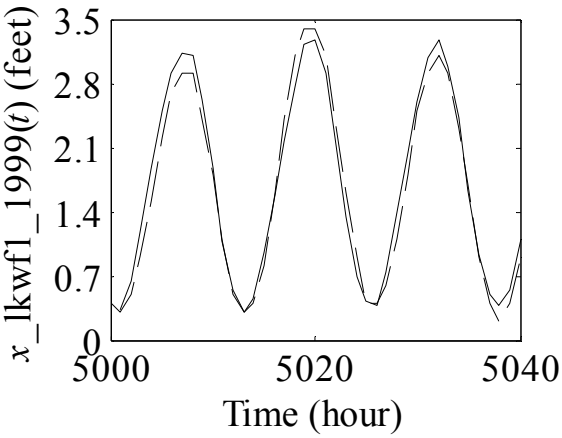

Figure 11. Prediction results with the sample size 900 at the Station LKWF1 in 1999. Solid line: predicted values, dashed line: original values.

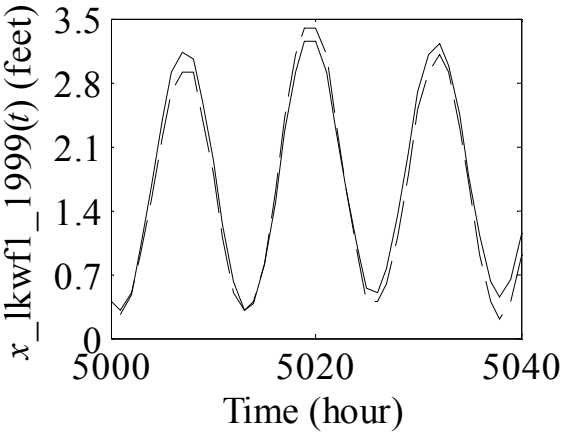

Figure 12. Prediction results with the sample size 1000 at the Station LKWF1 in 1999. Solid line: predicted values, dashed line: original values.

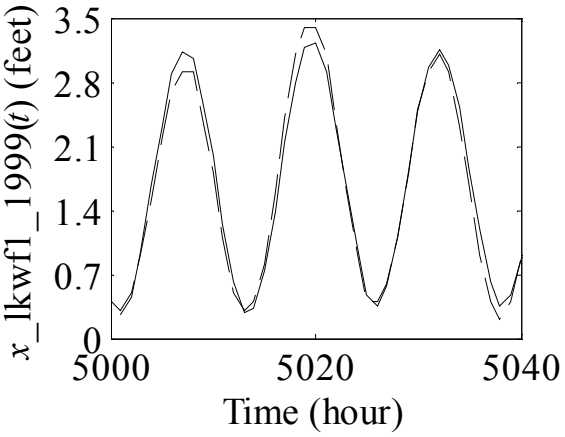

Figure 13. Prediction results with the sample size 1100 at the Station LKWF1 in 1999. Solid line: predicted values, dashed line: original values.

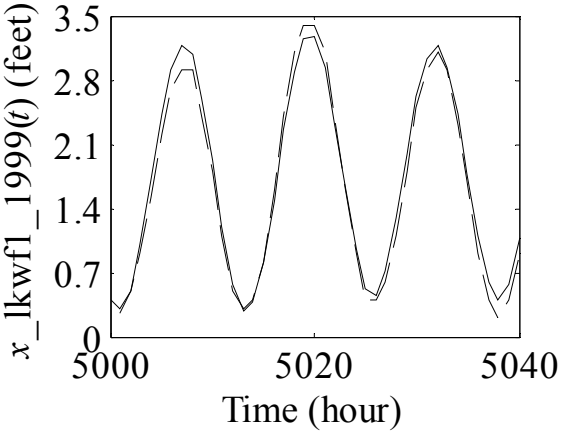

Figure 14. Prediction results with the sample size 1200 at the Station LKWF1 in 1999. Solid line: predicted values, dashed line: original values.

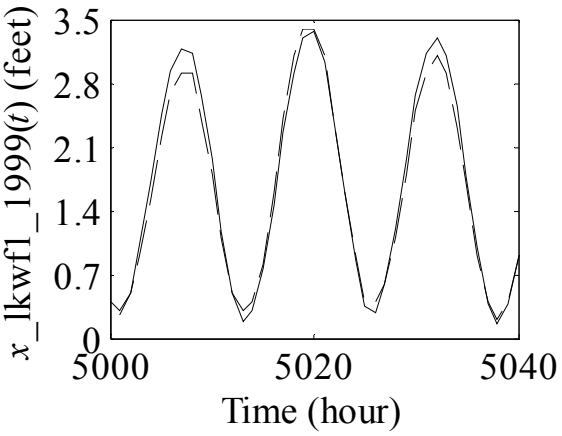

Figure 15. Prediction results with the sample size 1300 at the Station LKWF1 in 1999. Solid line: predicted values, dashed line: original values.

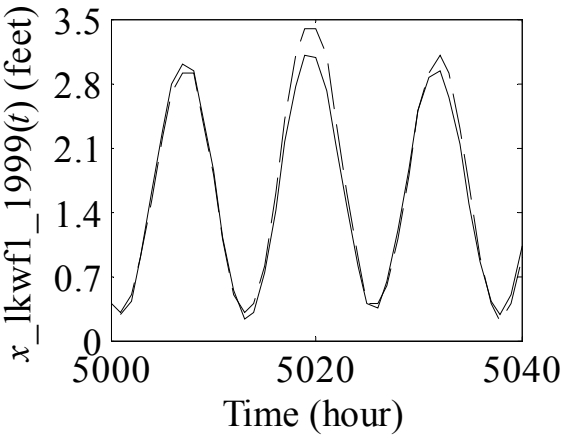

Figure 16. Prediction results with the sample size 1400 at the Station LKWF1 in 1999. Solid line: predicted values, dashed line: original values.

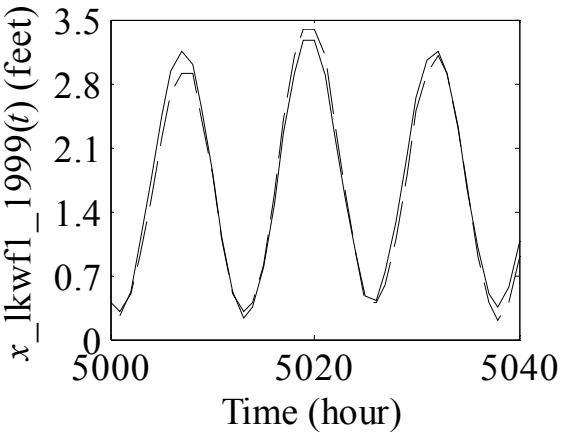

Figure 17. Prediction results with the sample size 1500 at the Station LKWF1 in 1999. Solid line: predicted values, dashed line: original values.

The values of prediction errors are summarized in Table 2. The relationship between the past sample size and prediction error is demonstrated by Figure 18, of which the generation process is shown in Figure 19.

Table 2. Prediction errors investigated using x_lkwf1_1999(t) in the Station LKWF1.

Past sample size: n	Number of data to be predicted: m	Past samples used	Predicted data	MSE: $e^2(n, m)$
100	40	4901st–5000th/ 4:00, 26 July–7:00, 30 July	8:00, 30 Jul.–23:00, 31 Jul.	0.38664
200	40	4801st–5000th/ 23:00, 21 Jul.–7:00, 30 Jul.	8:00, 30 Jul.–23:00, 31 Jul.	0.17422
300	40	4701st–5000th/ 19:00, 17 Jul.–7:00, 30 Jul.	8:00, 30 Jul.–23:00, 31 Jul.	0.09026
400	40	4601st–5000th/ 15:00, 13 Jul.–7:00, 30 Jul.	8:00, 30 Jul.–23:00, 31 Jul.	0.09519
500	40	4501st–5000th/ 10:00, 9 Jul.–7:00, 30 Jul.	8:00, 30 Jul.–23:00, 31 Jul.	0.06699
600	40	4401st–5000th/ 5:00, 5 Jul.–7:00, 30 Jul.	8:00, 30 Jul.–23:00, 31 Jul.	0.04418
700	40	4301st–5000th/ 1:00, 1 Jul.–7:00, 30 Jul.	8:00, 30 Jul.–23:00, 31 Jul.	0.04385
800	40	4201st–5000th/ 21:00, 26 Jun.–7:00, 30 Jul.	8:00, 30 Jul.–23:00, 31 Jul.	0.03291
900	40	4101st–5000th/ 17:00, 22 Jun.–7:00, 30 Jul.	8:00, 30 Jul.–23:00, 31 Jul.	0.02826
1000	40	4001st–5000th/ 13:00, 18 Jun.–7:00, 30 Jul.	8:00, 30 Jul.–23:00, 31 Jul.	0.02601
1100	40	3901st–5000th/ 9:00, 14 Jun.–7:00, 30 Jul.	8:00, 30 Jul.–23:00, 31 Jul.	0.02185
1200	40	3801st–5000th/ 5:00, 10 Jun.–7:00, 30 Jul.	8:00, 30 Jul.–23:00, 31 Jul.	0.02012
1300	40	3701st–5000th/ 20:00, 5 Jun.–7:00, 30 Jul.	8:00, 30 Jul.–23:00, 31 Jul.	0.02028
1400	40	3601st–5000th/ 16:00, 1 Jun.–7:00, 30 Jul.	8:00, 30 Jul.–23:00, 31 Jul.	0.02313
1500	40	3501st–5000th/ 12:00, 28 May–7:00, 30 Jul.	8:00, 30 Jul.–23:00, 31 Jul.	0.01762

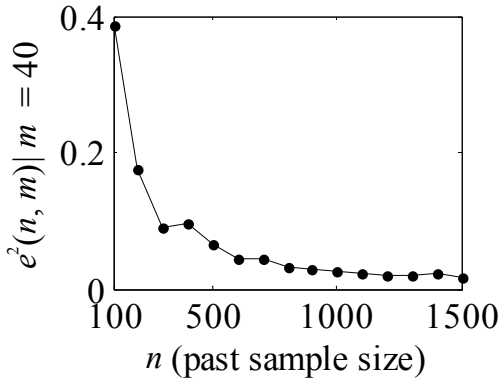

Figure 18. Relationship between the prediction error and the past sample size at the Station LKWF1 in 1999.

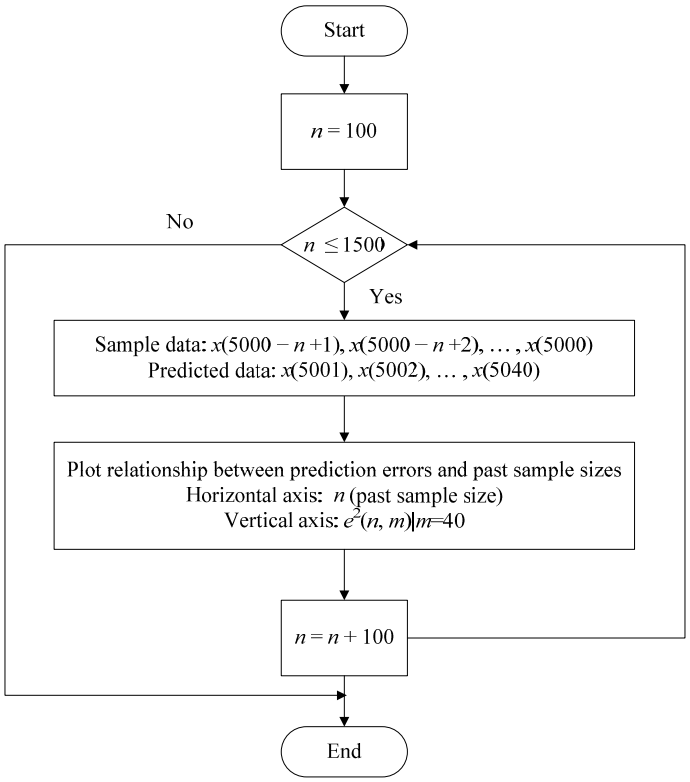

Figure 19. Generation process of relationship between prediction errors and past sample sizes.

Note 2. *From Figure 18, as well as Figure 20, we see that MSE decreases rapidly when the past sample size increases from 100 to 300. Then, prediction errors appear to decay slowly when the past sample size increases. Table 3 summarizes the results.*

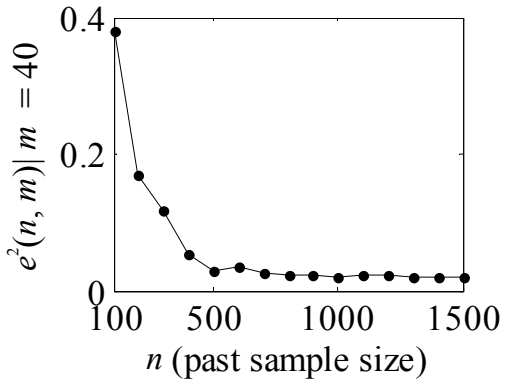

Figure 20. Relationship between the prediction error and the past sample size at the Station SMKF1 in 2003.

Table 3. Prediction errors investigated using x_smkf1_2003(t) in the Station SMKF1.

Past sample size: n	Number of data to be predicted: m	Past samples used	Predicted data	MSE: $e^2(n, m)$
100	40	4901st–5000th/ 13:00, 24 Jul.–16:00, 28 Jul.	17:00, 28 Jul.–8:00, 30 Jul.	0.37867
200	40	4801st–5000th/ 9:00, 20 Jul.–16:00, 28 Jul.	17:00, 28 Jul.–8:00, 30 Jul.	0.16937
300	40	4701st–5000th/ 5:00, 16 Jul.–16:00, 28 Jul.	17:00, 28 Jul.–8:00, 30 Jul.	0.11727
400	40	4601st–5000th/ 0:00, 12 Jul.–16:00, 28 Jul.	17:00, 28 Jul.–8:00, 30 Jul.	0.05214
500	40	4501st–5000th/ 20:00, 7 Jul.–16:00, 28 Jul.	17:00, 28 Jul.–8:00, 30 Jul.	0.02879
600	40	4401st–5000th/ 16:00, 3 Jul.–7:00, 30 Jul.	17:00, 28 Jul.–8:00, 30 Jul.	0.03622
700	40	4301st–5000th/ 12:00, 29 Jun.–16:00, 28 Jul.	17:00, 28 Jul.–8:00, 30 Jul.	0.02651
800	40	4201st–5000th/ 8:00, 25 Jun.–16:00, 28 Jul.	17:00, 28 Jul.–8:00, 30 Jul.	0.02235
900	40	4101st–5000th/ 4:00, 21 Jun.–16:00, 28 Jul.	17:00, 28 Jul.–8:00, 30 Jul.	0.02442
1000	40	4001st–5000th/ 0:00, 17 Jun.–16:00, 28 Jul.	17:00, 28 Jul.–8:00, 30 Jul.	0.02077
1100	40	3901st–5000th/ 20:00, 12 Jun.–16:00, 28 Jul.	17:00, 28 Jul.–8:00, 30 Jul.	0.02426
1200	40	3801st– 5000th/ 16:00, 8 Jun.–16:00, 28 Jul.	17:00, 28 Jul.–8:00, 30 Jul.	0.02265
1300	40	3701st–5000th/ 11:00, 4 Jun.–16:00, 28 Jul.	17:00, 28 Jul.–8:00, 30 Jul.	0.02037
1400	40	3601st–5000th/ 7:00, 31 May–16:00, 28 Jul.	17:00, 28 Jul.–8:00, 30 Jul.	0.02085
1500	40	3501st–5000th/ 3:00, 27 May–16:00, 28 Jul.	17:00, 28 Jul.–8:00, 30 Jul.	0.01981

Prediction results at the stations LONF1, SAUF1, SPGF1 and VENF1 are summarized (see Tables 4–7). The corresponding figures are also as follows (see Figures 21–24). Ignoring decay rates of the six stations, all the figures indicate that the prediction errors taper off on the whole as sample sizes increase, and curves decay fast at first but slowly in the end. When the sample size rises to a certain extent, the prediction accuracy cannot be obviously improved. That is to say, if the range of prediction errors has been determined, there is no need to take very large sample size. In the next section, we will fit the curve to explore the precise relationship between prediction errors and sample sizes.

Table 4. Prediction errors investigated using x_lonf1_2003(t) in the Station LONF1.

Past sample size: n	Number of data to be predicted: m	Past samples used	Predicted data	MSE: $e^2(n, m)$
100	40	4901st–5000th/18:00, 28 Jul.–21:00, 1 Aug.	22:00, 1 Aug.–13:00, 3 Aug.	0.15316
200	40	4801st–5000th/14:00, 24 Jul.–21:00, 1 Aug.	22:00, 1 Aug.–13:00, 3 Aug.	0.13100
300	40	4701st–5000th/10:00, 20 Jul.–21:00, 1 Aug.	22:00, 1 Aug.–13:00, 3 Aug.	0.12900
400	40	4601st–5000th/5:00, 16 Jul.–21:00, 1 Aug.	22:00, 1 Aug.–13:00, 3 Aug.	0.11930
500	40	4501st–5000th/1:00, 12 Jul.–21:00, 1 Aug.	22:00, 1 Aug.–13:00, 3 Aug.	0.10686
600	40	4401st–5000th/21:00, 7 Jul.–21:00, 1 Aug.	22:00, 1 Aug.–13:00, 3 Aug.	0.10962
700	40	4301st–5000th/17:00, 3 Jul.–21:00, 1 Aug.	22:00, 1 Aug.–13:00, 3 Aug.	0.10348
800	40	4201st–5000th/13:00, 29 Jun.–21:00, 1 Aug.	22:00, 1 Aug.–13:00, 3 Aug.	0.10434
900	40	4101st–5000th/4:00, 21 Jun.–21:00, 1 Aug.	22:00, 1 Aug.–13:00, 3 Aug.	0.10594
1000	40	4001st–5000th/9:00, 25 Jun.–21:00, 1 Aug.	22:00, 1 Aug.–13:00, 3 Aug.	0.10692
1100	40	3901st–5000th/23:00, 16 Jun.–21:00, 1 Aug.	22:00, 1 Aug.–13:00, 3 Aug.	0.10334
1200	40	3801st–5000th/19:00, 12 Jun.–21:00, 1 Aug.	22:00, 1 Aug.–13:00, 3 Aug.	0.09628
1300	40	3701st–5000th/15:00, 8 Jun.–21:00, 1 Aug.	22:00, 1 Aug.–13:00, 3 Aug.	0.09980
1400	40	3601st–5000th/11:00, 4 Jun.–21:00, 1 Aug.	22:00, 1 Aug.–13:00, 3 Aug.	0.10160
1500	40	3501st–5000th/16:00, 28 May–21:00, 1 Aug.	22:00, 1 Aug.–13:00, 3 Aug.	0.09752

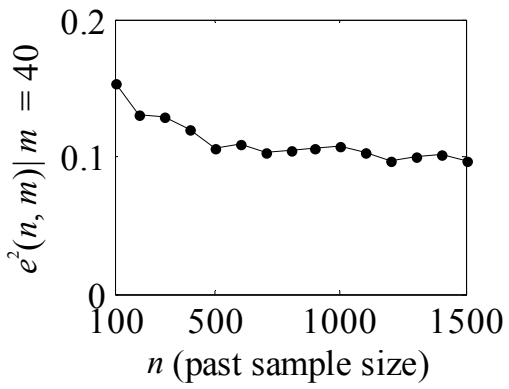

Figure 21. Relationship between the prediction error and the past sample size at the Station LONF1 in 2003.

Table 5. Prediction errors investigated using x_sauf1_2001(t) in the Station SAUF1.

Past sample size: n	Number of data to be predicted: m	Past samples used	Predicted data	MSE: $e^2(n, m)$
100	40	4901st–5000th/21:00, 28 Jul.–8:00, 2 Aug.	9:00, 2 Aug.–0:00, 4 Aug.	3.80104
200	40	4801st–5000th/16:00, 24 Jul.–8:00, 2 Aug.	9:00, 2 Aug.–0:00, 4 Aug.	2.56308
300	40	4701st–5000th/12:00, 20 Jul.–8:00, 2 Aug.	9:00, 2 Aug.–0:00, 4 Aug.	1.45882
400	40	4601st–5000th/3:00, 16 Jul.–8:00, 2 Aug.	9:00, 2 Aug.–0:00, 4 Aug.	1.28306
500	40	4501st–5000th/21:00, 11 Jul.–8:00, 2 Aug.	9:00, 2 Aug.–0:00, 4 Aug.	0.96792
600	40	4401st–5000th/17:00, 7 Jul.–8:00, 2 Aug.	9:00, 2 Aug.–0:00, 4 Aug.	0.95034
700	40	4301st–5000th/11:00, 3 Jul.–8:00, 2 Aug.	9:00, 2 Aug.–0:00, 4 Aug.	0.89086
800	40	4201st–5000th/7:00, 29 Jun.–8:00, 2 Aug.	9:00, 2 Aug.–0:00, 4 Aug.	0.63288
900	40	4101st–5000th/3:00, 25 Jun.–8:00, 2 Aug.	9:00, 2 Aug.–0:00, 4 Aug.	0.61248
1000	40	4001st–5000th/21:00, 20 Jun.–8:00, 2 Aug.	9:00, 2 Aug.–0:00, 4 Aug.	0.48420
1100	40	3901st–5000th/16:00, 16 Jun.–8:00, 2 Aug.	9:00, 2 Aug.–0:00, 4 Aug.	0.41888
1200	40	3801st–5000th/12:00, 12 Jun.–8:00, 2 Aug.	9:00, 2 Aug.–0:00, 4 Aug.	0.33480
1300	40	3701st–5000th/7:00, 8 Jun.–8:00, 2 Aug.	9:00, 2 Aug.–0:00, 4 Aug.	0.33480
1400	40	3601st–5000th/3:00, 4 Jun.–8:00, 2 Aug.	9:00, 2 Aug.–0:00, 4 Aug.	0.33488
1500	40	3501st – 5000th/23:00, 30 May – 8:00, 2 Aug.	9:00, 2 Aug.–0:00, 4 Aug.	0.32614

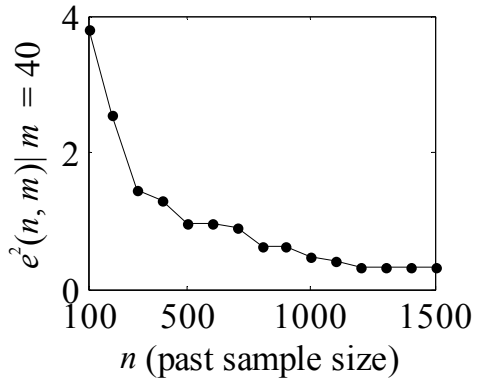

Figure 22. Relationship between the prediction error and the past sample size at the Station SAUF1 in 2001.

Table 6. Prediction errors investigated using x_spgf1_1996(t) in the Station SPGF1.

Past sample size: n	Number of data to be predicted: m	Past samples used	Predicted data	MSE: $e^2(n, m)$
100	40	4901st–5000th/3:00, 21 Jul.–7:00, 25 Jul.	8:00, 25 Jul.–23:00, 26 Jul.	0.38766
200	40	4801st–5000th/23:00, 16 Jul.–7:00, 25 Jul.	8:00, 25 Jul.–23:00, 26 Jul.	0.18390
300	40	4701st–5000th/14:00, 12 Jul.–7:00, 25 Jul.	8:00, 25 Jul.–23:00, 26 Jul.	0.15660
400	40	4601st–5000th/8:00, 8 Jul.–7:00, 25 Jul.	8:00, 25 Jul.–23:00, 26 Jul.	0.14834
500	40	4501st–5000th/2:00, 4 Jul.–7:00, 25 Jul.	8:00, 25 Jul.–23:00, 26 Jul.	0.13988
600	40	4401st–5000th/21:00, 4 Jul.–7:00, 25 Jul.	8:00, 25 Jul.–23:00, 26 Jul.	0.11374
700	40	4301st–5000th/14:00, 29 Jun.–7:00, 25 Jul.	8:00, 25 Jul.–23:00, 26 Jul.	0.10464
800	40	4201st–5000th/10:00, 25 Jun.–7:00, 25 Jul.	8:00, 25 Jul.–23:00, 26 Jul.	0.08100
900	40	4101st–5000th/6:00, 21 Jun.–7:00, 25 Jul.	8:00, 25 Jul.–23:00, 26 Jul.	0.07846
1000	40	4001st–5000th/1:00, 17 Jun.–7:00, 25 Jul.	8:00, 25 Jul.–23:00, 26 Jul.	0.07160
1100	40	3901st–5000th/20:00, 12 Jun.–7:00, 25 Jul.	8:00, 25 Jul.–23:00, 26 Jul.	0.06674
1200	40	3801st–5000th/16:00, 8 Jun.–7:00, 25 Jul.	8:00, 25 Jul.–23:00, 26 Jul.	0.06592
1300	40	3701st–5000th/11:00, 4 Jun.–7:00, 25 Jul.	8:00, 25 Jul.–23:00, 26 Jul.	0.06926
1400	40	3601st–5000th/7:00, 31 May–7:00, 25 Jul.	8:00, 25 Jul.–23:00, 26 Jul.	0.06532
1500	40	3501st–5000th/2:00, 27 May–7:00, 25 Jul.	8:00, 25 Jul.–23:00, 26 Jul.	0.06512

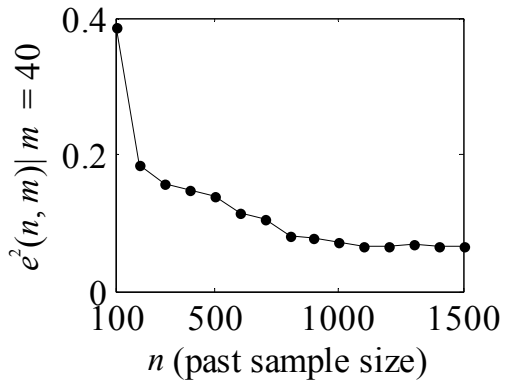

Figure 23. Relationship between the prediction error and the past sample size at the Station SPGF1 in 1996.

Table 7. Prediction errors investigated using x_venf1_2003(t) in the Station VENF1.

Past sample size: n	Number of data to be predicted: m	Past samples used	Predicted data	MSE: $e^2(n, m)$
100	40	4901st–5000th/20:00, 24 Jul.–23:00 28 Jul.	0:00, 29 Jul.–15:00, 30 Jul.	0.44356
200	40	4801st–5000th/16:00, 20 Jul.–23:00, 28 Jul.	0:00, 29 Jul.–15:00, 30 Jul.	0.12978
300	40	4701st–5000th/12:00, 16 Jul.–23:00, 28 Jul.	0:00, 29 Jul.–15:00, 30 Jul.	0.08738
400	40	4601st–5000th/8:00, 12 Jul.–23:00, 28 Jul.	0:00, 29 Jul.–15:00, 30 Jul.	0.04698
500	40	4501st–5000th/23:00, 7 Jul.–23:00, 28 Jul.	0:00, 29 Jul.–15:00, 30 Jul.	0.03906
600	40	4401st–5000th/19:00, 3 Jul.–23:00, 28 Jul.	0:00, 29 Jul.–15:00, 30 Jul.	0.03502
700	40	4301st–5000th/15:00, 29 Jun.–23:00, 28 Jul.	0:00, 29 Jul.–15:00, 30 Jul.	0.02538
800	40	4201st–5000th/10:00, 25 Jun.–23:00, 28 Jul.	0:00, 29 Jul.–15:00, 30 Jul.	0.02060
900	40	4101st–5000th/6:00, 21 Jun.–23:00, 28 Jul.	0:00, 29 Jul.–15:00, 30 Jul.	0.01870
1000	40	4001st–5000th/2:00, 17 Jun.–23:00, 28 Jul.	0:00, 29 Jul.–15:00, 30 Jul.	0.01878
1100	40	3901st–5000th/22:00, 12 Jun.–23:00, 28 Jul.	0:00, 29 Jul.–15:00, 30 Jul.	0.01894
1200	40	3801st–5000th/18:00, 8 Jun.–23:00, 28 Jul.	0:00, 29 Jul.–15:00, 30 Jul.	0.01672
1300	40	3701st–5000th/14:00, 4 Jun.–23:00, 28 Jul.	0:00, 29 Jul.–15:00, 30 Jul.	0.01594
1400	40	3601st–5000th/10:00, 31 May–23:00, 28 Jul.	0:00, 29 Jul.–15:00, 30 Jul.	0.01716
1500	40	3501st–5000th/5:00, 27 May–23:00, 28 Jul.	0:00, 29 Jul.–15:00, 30 Jul.	0.01888

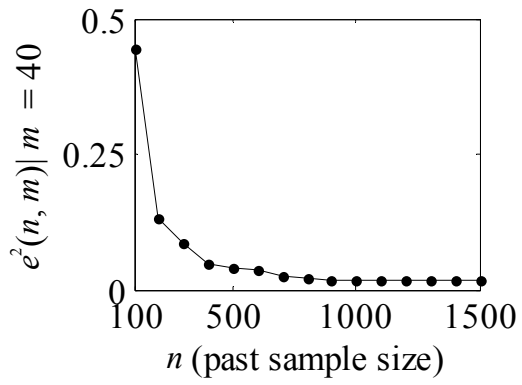

Figure 24. Relationship between the prediction error and the past sample size at the Station VENF1 in 2003.

4.2. Prediction Error Curve Fitting

Data fitting is used to select the proper type of curve to fit the observed data, and analyze the relationship between these two variables based on the curve fitting equation. In this paper, power function satisfactorily fits the prediction error curve according to the shape characteristic of the curve. Figures 25–30 show the prediction errors' fitting results of the six aforementioned stations. The corresponding power functions are also listed in Table 8.

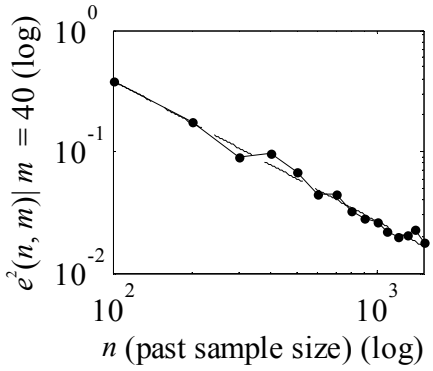

Figure 25. Curve fitting of the Station LKWF1 in 1999. Solid line: original curve, dashed line: fitting curve.

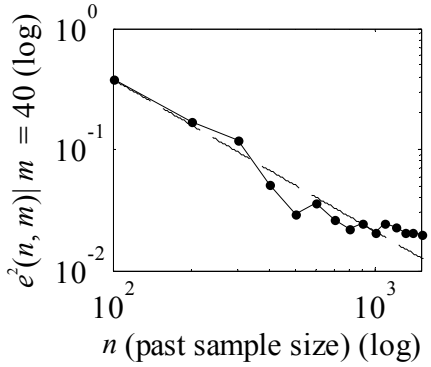

Figure 26. Curve fitting of the Station SMKF1 in 2003. Solid line: original curve, dashed line: fitting curve.

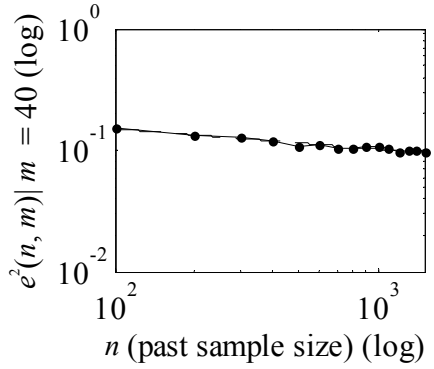

Figure 27. Curve fitting of the Station LONF1 in 2003. Solid line: original curve, dashed line: fitting curve.

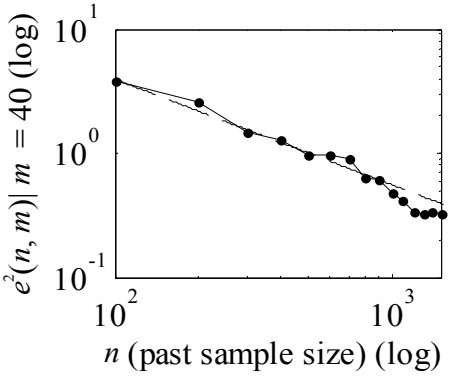

Figure 28. Curve fitting of the Station SAUF1 in 2001. Solid line: original curve, dashed line: fitting curve.

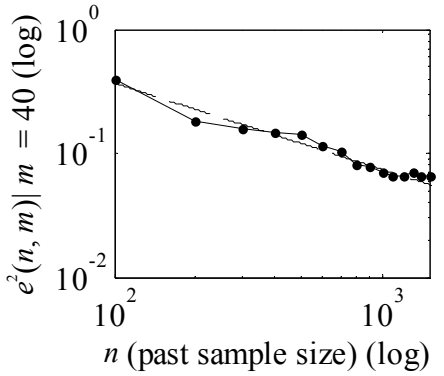

Figure 29. Curve fitting of the Station SPGF1 in 1996. Solid line: original curve, dashed line: fitting curve.

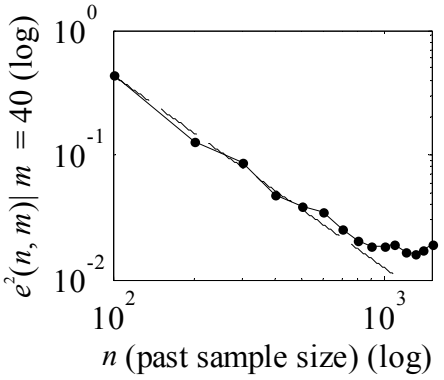

Figure 30. Curve fitting of the Station VENF1 in 2003. Solid line: original curve, dashed line: fitting curve.

Table 8. Curve fitting results of the six stations. $f(n) = e^2(n, m)|m = 40$, n is the past sample size.

Station name	Power functions
LKWF1	$f(n) = 78.680n^{-1.1550}$
SMKF1	$f(n) = 121.600n^{-1.252}$
LONF1	$f(n) = 0.3194n^{-0.1645}$
SAUF1	$f(n) = 195.50n^{-0.8476}$
SPGF1	$f(n) = 9.0370n^{-0.6948}$
VENF1	$f(n) = 562.50n^{-1.5400}$

Both figures and table indicate that prediction errors at different stations have the same function form in power law. Power functions fit prediction error curves satisfactorily. The quantitative functions may help us determine the range of sample size in the case that prediction accuracy is ensured, which improves utilization of data.

The above experimental results with respect to prediction errors are expressed as

$$f(n) = An^{-a}, \quad A > 0, a > 0. \tag{8}$$

According to the physical meaning of past sample size, we have $n > 0$. Thus, by denoting $H(n)$ the Heaviside unit step function, we rewrite Equation (8) as

$$f(n) = An^{-a}H(n), \quad A > 0, a > 0. \tag{9}$$

The above expression may serve as a solution to the problem we raised in Section 2.

Note 2. *The prediction error f(n) provides us with a guideline to control the prediction error in terms of a given value of past sample size.*

Note 3. *Our present result about f(n) may serve as a specific case for the quantitative description of prediction error for that* $f(n) \to 0$ *for* $n \to \infty$*, which was qualitatively described by Kolmogorov, see Corollary 1.*

4.3. Discussions

Sea level time series has the property of long-range dependence (LRD), as can be seen from Ercan *et al.* [90], Barbosa *et al.* [91], Beretta *et al.* [92], and Li *et al.* [93]. Denote by $y(t)$ a time series in general. Its autocorrelation function (ACF) is denote by $r_{yy}(\tau) = \mathrm{E}[y(t)y(t + \tau)]$. By LRD (Beran [94]), we mean

$$\int_0^\infty r_{yy}(\tau)d\tau = \infty. \tag{10}$$

A typical case of $r_{yy}(\tau)$, which satisfies the above, is a decayed power function expressed as

$$r_{yy}(\tau) \sim c\tau^{-b} (0 < b < 1), \tag{11}$$

where $b = 2 - 2H$, $H \in (0.5, 1)$ is the Hurst parameter. Time series with LRD, in addition to sea level time series, have wide applications in various fields, ranging from physics to computer science, see e.g., [95–124], just mentioning a few with the preference by Mandelbrot [125] and references therein, where H plays a key role. At the moment, however, we have not got enough knowledge to establish the relationship between H and the past sample size with respect to prediction errors of sea level time series.

Our future work will work at it so as to understand deeply the issue of prediction errors of sea level time series. Another future work of ours is to investigate whether power-type functions of prediction error might appear as a law in the aspect of prediction of time series with LRD in general besides sea level time series.

As previously mentioned in the Introduction, there are two categories of predictors, namely, linear predictors and nonlinear ones [2–23,32–70,73–89], which may be considered for a specific type of time series, such as sea level. Since sea level is of LRD [90–93], which is nonlinear, and since, ANN is a nonlinear predictor, it was consequently used in this research.

In the future, we shall use other types of predictors, for instance, autoregressive (AR) type, to study the relationship between prediction error and past sample size of sea level time series, and compare it with the one presented in this research.

Note that the present relationship between prediction error and past sample size may be a law specifically for sea level time series. In general, we never imply that it may fit with other types of time series, such as ocean surface waves or network traffic. Nevertheless, it might yet be a reference for them in this regard.

Finally, we note that this research is in the domain of statistics. Therefore, though the data used in this research (see Table 1) are from 1999 to 2003, we statistically infer that the present law is available for hourly recorded sea level in the past and future.

6. Conclusions

We have established the relationship between prediction error and past sample size for the prediction of sea level time series based on real data measured at six stations on the east coast of the Gulf of Mexico in Florida. The closed form of that relationship, in decayed power functions, has been obtained. It may yet be useful, on the one hand, for one to control prediction error according to a given past sample size or, on the other hand, for us to require the size of past sample according to a predetermined prediction error.

Sea water levels at six stations on the east coast of the Gulf of Mexico, Florida are predicted. A type of artificial neural network, back propagation (BP), is used with the Neural Network Toolbox in MATLAB. Prediction errors with different values are generated according to changes in sample sizes.

Acknowledgments

This paper was partly supported by the National Natural Science Foundation of China under the Project Grant Nos. 61272402 and 61070214. We appreciate the National Data Buoy Center that provides its measured data of sea level, which makes our research possible.

Conflicts of Interest

The authors declare that there is no conflict of interests regarding the publication of this paper.

References

1. Sampaio, L.E.B.; Rezende, A.L.T.; Nieckele, A.O. The challenging case of the turbulent flow around a thin plate wind deflector, and its numerical prediction by LES and RANS models. *J. Wind Eng. Ind. Aerodyn.* **2014**, *133*, 52–64.

2. Sanayei, M.; Moore, J.A.; Brett, C.R. Measurement and prediction of train-induced vibrations in a full-scale building. *Eng. Struct.* **2014**, *77*, 119–128.
3. Tsai, J.S.-H.; Hsu, W.-T.; Wei, C.-L.; Guo, S.-M.; Shieh, L.-S. Universal prediction-based adaptive fault estimator applied to secure communication. *Appl. Math. Model.* **2014**, *38*, 4717–4732.
4. Millán, M.M. Extreme hydrometeorological events and climate change predictions in Europe. *J. Hydrol.* **2014**, *518*, 206–224.
5. Schijve, J. The significance of fatigue crack initiation for predictions of the fatigue limit of specimens and structures. *Int. J. Fatigue* **2014**, *61*, 39–45.
6. Zhao, X.; Dryer, M. Current status of CME/shock arrival time prediction. *Space Weather* **2014**, *12*, 448–469.
7. Stockdon, H.; Thompson, D.; Plant, N.; Long, J. Evaluation of wave runup predictions from numerical and parametric models. *Coasta. Eng.* **2014**, *92*, 1–11.
8. Dimberg, P.H.; Bryhn, A.C. Predicted effects from abatement action against eutrophication in two small bays of the Baltic Sea. *Environ. Earth Sci.* **2014**, *72*, 1191–1199.
9. Hackert, E.; Busalacchi, A.J.; Ballabrera-Poy, J. Impact of Aquarius sea surface salinity observations on coupled forecasts for the tropical Indo-Pacific Ocean. *J. Geophys. Res. Ocean.* **2014**, *119*, 4045–4067.
10. Barik, A.K.; Dash, S.K.; Guha, A. New correlation for prediction of air entrainment into an Infrared Suppression (IRS) device. *Appl. Ocean Res.* **2014**, *47*, 303–312.
11. Luhar, M.; Sharma, A.; McKeon, B. On the structure and origin of pressure fluctuations in wall turbulence: Predictions based on the resolvent analysis. *J. Fluid Mech.* **2014**, *751*, 38–70.
12. Bagheripour, P.; Asoodeh, M. Poisson's ratio prediction through dual stimulated fuzzy logic by ACE and GA-PS. *J. Appl. Geophys.* **2014**, *107*, 55–59.
13. Camus, P.; Méndez, F.J.; Losada, I.J.; Menéndez, M.; Espejo, A.; Pérez, J.; Rueda, A.; Guanche, Y. A method for finding the optimal predictor indices for local wave climate conditions. *Ocean Dyn.* **2014**, *64*, 1025–1038.
14. Hüffer, T.; Endo, S.; Metzelder, F.; Schroth, S.; Schmidt, T.C. Prediction of sorption of aromatic and aliphatic organic compounds by carbon nanotubes using poly-parameter linear free-energy relationships. *Water Res.* **2014**, *59*, 295–303.
15. Frousios, K.; Iliopoulos, C.S.; Schlitt, T.; Simpson, M.A. Predicting the functional consequences of non-synonymous DNA sequence variants—evaluation of bioinformatics tools and development of a consensus strategy. *Genomics* **2013**, *102*, 223–228.
16. Pike, A.; Danner, E.; Boughton, D.; Melton, F.; Nemani, R.; Rajagopalan, B.; Lindley, S. Forecasting river temperatures in real time using a stochastic dynamics approach. *Water Resour. Res.* **2013**, *49*, 5168–5182.
17. Duan, W.-Q.; Stanley, H.E. Cross-correlation and the predictability of financial return series. *Physica A* **2011**, *390*, 290–296.
18. Duan, W.-Q.; Stanley, H.E. Volatility, irregularity, and predictable degree of accumulative return series. *Phys. Rev. E* **2010**, *81*, 066116.
19. Kumar, P.; Franzese, G.; Stanley, H.E. Predictions of dynamic behavior under pressure for two scenarios to explain water anomalies. *Phys. Rev. Lett.* **2008**, *100*, 105701.

20. Starr, F.W.; Angell, C.A.; Stanley, H.E. Prediction of entropy and dynamic properties of water below the homogeneous nucleation temperature. *Physica A* **2003**, *323*, 51–66.
21. Niedzielski, T.; Miziński, B. Automated system for near-real time modelling and prediction of altimeter-derived sea level anomalies. *Comput. Geosci.* **2013**, *58*, 29–39.
22. Nitsure, S.; Londhe, S.; Khare, K. Prediction of sea water levels using wind information and soft computing techniques. *Appl. Ocean Res.* **2014**, *47*, 344–351.
23. Santoro, P.; Fernández, M.; Fossati, M.; Cazes, G.; Terra, R.; Piedra-Cueva, I. Pre-operational forecasting of sea level height for the Río de la Plata. *Appl. Math. Model.* **2011**, *35*, 2462–2478.
24. Gardner, A.S.; Moholdt, G.; Cogley, J.G.; Wouters, B.; Arendt, A.A.; Wahr, J.; Berthier, E.; Hock, R.; Pfeffer, W.T.; Kaser, G. A reconciled estimate of glacier contributions to sea level rise: 2003 to 2009. *Science* **2013**, *340*, 852–857.
25. Graham, S.; Barnett, J.; Fincher, R.; Hurlimann, A.; Mortreux, C.; Waters, E. The social values at risk from sea-level rise. *Environ. Impact Assess. Rev.* **2013**, *41*, 45–52.
26. Kamb, B. Glacier Geophysics Dynamic response of glaciers to changing climate may shed light on processes in the earth's interior. *Science* **1964**, *146*, 353–365.
27. Kim, Y.C. *Handbook of Coastal and Ocean Engineering*; World Scientific: Singapore, Singapore, 2010.
28. Massel, S.R. *Ocean Surface Waves: Their Physics and Prediction*; World Scientific: Singapore, Singapore, 1996.
29. Mudersbach, C.; Wahl, T.; Haigh, I.D.; Jensen, J. Trends in high sea levels of German North Sea gauges compared to regional mean sea level changes. *Cont. Shelf Res.* **2013**, *65*, 111–120.
30. Oliver, E.; Thompson, K. Madden-Julian Oscillation and sea level: Local and remote forcing. *J. Geophys. Res. Oceans* **2010**, *115*, doi:10.1029/2009JC005337.
31. Parker, A. Impacts of sea level rise on coastal planning in Norway. *Ocean Eng.* **2014**, *78*, 124–130.
32. Atal, B.S. The history of linear prediction. *IEEE Signal Process. Mag.* **2006**, *23*, 154–161.
33. Carotti, E.S.; De Martin, J.C.; Merletti, R.; Farina, D. Compression of multidimensional biomedical signals with spatial and temporal codebook-excited linear prediction. *IEEE Trans. Biomed. Eng.* **2009**, *56*, 2604–2610.
34. Kugiumtzis, D.; Lingjærde, O.; Christophersen, N. Regularized local linear prediction of chaotic time series. *Physica D* **1998**, *112*, 344–360.
35. Lawrence, M.; Goodwin, P.; O'Connor, M.; Önkal, D. Judgmental forecasting: A review of progress over the last 25years. *Int. J. Forecast.* **2006**, *22*, 493–518.
36. Lyman, R.J.; Edmonson, W.W. Linear prediction of bandlimited processes with flat spectral densities. *IEEE Trans. Signal Process.* **2001**, *49*, 1564–1569.
37. Man, K.S. Linear prediction of temporal aggregates under model misspecification. *Int. J. Forecast.* **2004**, *20*, 659–670.
38. Mugler, D.H. Computationally efficient linear prediction from past samples of a band-limited signal and its derivative. *IEEE Trans. Inf. Theory* **1990**, *36*, 589–596.
39. Navarro-Moreno, J.; Moreno-Kaiser, J.; Fernández-Alcalá, R.M.; Ruiz-Molina, J.C. Widely linear prediction for transfer function models based on the infinite past. *Comput. Stat. Data Anal.* **2013**, *58*, 139–146.

40. Shin, H.; Hsing, T. Linear prediction in functional data analysis. *Stoch. Process. Appl.* **2012**, *122*, 3680–3700.
41. Tugnait, J.K.; Li, T.-T. A multistep linear prediction approach to blind asynchronous CDMA channel estimation and equalization. *IEEE J. Select. Areas Commun*. **2001**, *19*, 1090–1102.
42. Dhanya, C.; Nagesh Kumar, D. Nonlinear ensemble prediction of chaotic daily rainfall. *Adv. Water Res.* **2010**, *33*, 327–347.
43. Laio, F.; Porporato, A.; Revelli, R.; Ridolfi, L. A comparison of nonlinear flood forecasting methods. *Water Resour. Res.* **2003**, *39*, doi:10.1029/2002WR001551.
44. Sugihara, G. Nonlinear forecasting for the classification of natural time series. *Phil. Trans. R. Soc. Lond. A* **1994**, *348*, 477–495.
45. Yao, Q.; Tong, H. Quantifying the influence of initial values on non-linear prediction. *J. R. Stat. Soc. B* **2009**, *56*, 701–725.
46. Yilmaz, Y.; Kozat, S.S. Competitive randomized nonlinear prediction under additive noise. *IEEE Trans. Signal Process. Lett.* **2010**, *17*, 335–339.
47. Aladag, C.H.; Yolcu, U.; Egrioglu, E.; Bas, E. Fuzzy lagged variable selection in fuzzy time series with genetic algorithms. *Appl. Soft Comput.* **2014**, *22*, 465–473.
48. Egrioglu, E. PSO-based high order time invariant fuzzy time series method: Application to stock exchange data. *Econ. Model.* **2014**, *38*, 633–639.
49. Egrioglu, E.; Aladag, C.H.; Yolcu, U.; Uslu, V.R.; Basaran, M.A. Finding an optimal interval length in high order fuzzy time series. *Expert Syst. Appl.* **2010**, *37*, 5052–5055.
50. Egrioglu, E.; Yolcu, U.; Aladag, C.H.; Kocak, C. An ARMA type fuzzy time series forecasting method based on particle swarm optimization. *Math. Probl. Eng.* **2013**, *2013*, doi:10.1155/2013/935815.
51. Khoshnevisan, B.; Rafiee, S.; Omid, M.; Mousazadeh, H. Prediction of potato yield based on energy inputs using multi-layer adaptive neuro-fuzzy inference system. *Measurement* **2014**, *47*, 521–530.
52. Grivas, G.; Chaloulakou, A. Artificial neural network models for prediction of PM 10 hourly concentrations, in the Greater Area of Athens, Greece. *Atmos. Environ.* **2006**, *40*, 1216–1229.
53. Nastos, P.; Paliatsos, A.; Koukouletsos, K.; Larissi, I.; Moustris, K. Artificial neural networks modeling for forecasting the maximum daily total precipitation at Athens, Greece. *Atmos. Res.* **2014**, *144*, 141–150.
54. Momeni, E.; Nazir, R.; Armaghani, D.J.; Maizir, H. Prediction of pile bearing capacity using a hybrid genetic algorithm-based ANN. *Measurement* **2014**, *57*, 122–131.
55. Nastos, P.; Moustris, K.; Larissi, I.; Paliatsos, A. Rain intensity forecast using artificial neural networks in Athens, Greece. *Atmos. Res.* **2013**, *119*, 153–160.
56. Venkata Rao, K.; Murthy, B.; Mohan Rao, N. Prediction of cutting tool wear, surface roughness and vibration of work piece in boring of AISI 316 steel with artificial neural network. *Measurement* **2014**, *51*, 63–70.
57. Zanuttigh, B.; Formentin, S.M.; Briganti, R. A neural network for the prediction of wave reflection from coastal and harbor structures. *Coast. Eng.* **2013**, *80*, 49–67.
58. Yin, J.-C.; Zou, Z.-J.; Xu, F. On-line prediction of ship roll motion during maneuvering using sequential learning RBF neuralnetworks. *Ocean Eng.* **2013**, *61*, 139–147.

59. Kömürcü, M.İ.; Kömür, M.A.; Akpınar, A.; Özölçer, İ.H.; Yüksek, Ö. Prediction of offshore bar-shape parameters resulted by cross-shore sediment transport using neural network. *Appl. Ocean Res.* **2013**, *40*, 74–82.
60. Karakış, R.; Tez, M.; Kılıç, Y.A.; Kuru, Y.; Güler, İ. A genetic algorithm model based on artificial neural network for prediction of the axillary lymph node status in breastcancer. *Eng. Appl. Artif. Intell.* **2013**, *26*, 945–950.
61. Singh, U.K.; Tiwari, R.; Singh, S. Neural network modeling and prediction of resistivity structures using VES Schlumberger data over a geothermal area. *Comput. Geosci.* **2013**, *52*, 246–257.
62. Yang, W.; Xia, X. Prediction of mining subsidence under thin bedrocks and thick unconsolidated layers based on field measurement and artificial neural networks. *Comput. Geosci.* **2013**, *52*, 199–203.
63. Ceryan, N.; Okkan, U.; Kesimal, A. Prediction of unconfined compressive strength of carbonate rocks using artificial neural networks. *Environ. Earth Sci.* **2013**, *68*, 807–819.
64. Erzin, Y.; Cetin, T. The prediction of the critical factor of safety of homogeneous finite slopes using neural networks and multiple regressions. *Comput. Geosci.* **2013**, *51*, 305–313.
65. Wei, Y.; Chen, M.-C. Forecasting the short-term metro passenger flow with empirical mode decomposition and neural networks. *Transp. Res. C* **2012**, *21*, 148–162.
66. Liao, D.; Wang, Q.; Zhou, Y.; Liao, X.; Huang, C. Long-term prediction of the Earth Orientation Parameters by the artificial neural network technique. *J. Geodyn.* **2012**, *62*, 87–92.
67. Bowden, G.J.; Maier, H.R.; Dandy, G.C. Real-time deployment of artificial neural network forecasting models: Understanding the range of applicability. *Water Resour. Res.* **2012**, *48*, doi:10.1029/2012WR011984.
68. Blanco, A.M.; Sotto, A.; Castellanos, A. Prediction of the amount of wood using neural networks. *J. Math. Model. Algorithms* **2012**, *11*, 295–307.
69. Khashei, M.; Bijari, M. Hybridization of the probabilistic neural networks with feed-forward neural networks for forecasting. *Eng. Appl. Artif. Intell.* **2012**, *25*, 1277–1288.
70. Panella, M. Advances in biological time series prediction by neural networks. *Biomed. Signal Process. Control* **2011**, *6*, 112–120.
71. Gilhousen, D.B. A field evaluation of NDBC moored buoy winds. *J. Atmos. Ocean. Technol.* **1987**, *4*, 94–104.
72. Kolmogorov, A.N. On the representation of continuous functions of many variables by superposition of continuous functions of one variable and addition. *Am. Math. Soc. Transl*. **1963**, *28*, 55–59.
73. Hecht-Nielsen, R. Theory of the backpropagation neural network. In Proceedings of International Joint Conference on Neural Networks, Washington, DC, USA, 18–22 June 1989; pp. 593–605.
74. Zhang, Y.; Wu, L. Stock market prediction of S&P 500 via combination of improved BCO approach and BP neural network. *Expert Syst. Appl.* **2009**, *36*, 8849–8854.
75. Ciampi, A.; Zhang, F. A new approach to training back-propagation artificial neural networks: empirical evaluation on ten data sets from clinical studies. *Stat. Med.* **2002**, *21*, 1309–1330.
76. Guodong, L.; Jing, D. Discussion on problems of BP neural networks applied to hydrological prediction. *J. Hydraul. Eng.* **1999**, *1*, 66–71. (In Chinese)

77. Guo, Z.-H.; Wu, J.; Lu, H.-Y.; Wang, J.-Z. A case study on a hybrid wind speed forecasting method using BP neural network. *Knowl. -Based Syst.* **2011**, *24*, 1048–1056.
78. Huang, S.-C.; Huang, Y.-F. Bounds on the number of hidden neurons in multilayer perceptrons. *IEEE Trans. Neural Netw.* **1991**, *2*, 47–55.
79. Sheela, K.G.; Deepa, S. Review on methods to fix number of hidden neurons in neural networks. *Math. Probl. Eng.* **2013**, *2013*,doi:10.1155/2013/425740.
80. Hecht-Nielsen, R. Kolmogorov's mapping neural network existence theorem. In Proceedings of the First IEEE International Conference On Neural Networks, San Diego, CA, USA, 1987; pp. 11–14.
81. He, Y.-G.; Tan, Y.-H.; Sun, Y. A neural network approach for fault diagnosis of large-scale analogue circuits. *IEEE Int. Symp. Circuits Syst.* **2002**, *1*, 153–156.
82. Liu, X.; Chen, X.; Wu, W.; Peng, G. A neural network for predicting moisture content of grain drying process using genetic algorithm. *Food Control* **2007**, *18*, 928–933.
83. Jwo, D.-J.; Chin, K.-P. Applying back-propagation neural networks to GDOP approximation. *J. Navig.* **2002**, *55*, 97–108.
84. Sola, J.; Sevilla, J. Importance of input data normalization for the application of neural networks to complex industrial problems. *IEEE Trans. Nucl. Sci.* **1997**, *44*, 1464–1468.
85. Demuth, H.B.; Beale, M.H. Neural Network Toolbox for Use with MATLAB: Computation, Visualization, Programming-User's Guide; MathWorks: Natick, MA, USA, 2000.
86. Chen, W.; Ma, R.X.; Hao, Y.H. BP artificial neural network design based on MATLAB. *Comput. Study* **2005**, *2*, 30–31. (In Chinese)
87. Han, C.; Lv, Y.; Yang, D.; Hao, Y. An intrusion detection system based on neural network. In Proceedings of 2011 International Conference on Mechatronic Science, Electric Engineering and Computer, Jilin, China, 19–22 August 2011; pp. 2018–2021.
88. Affandi, A.K.; Watanabe, K.; Tirtomihardjo, H. Application of an artificial neural network to estimate groundwater level fluctuation. *J. Spat. Hydrol.* **2007**, *7*, 23–46.
89. Keyhani, R.; Deriche, M.; Palmer, E. A high impedance fault detector using a neural network and subband decomposition. In Proceedings of the Sixth International Symposium on Signal Processing and its Applications, Kuala Lumpur, Malaysia, 13–16 August 2001; pp. 458–461.
90. Ercan, A.; Kavvas, M.L.; Abbasov, R.K. *Long-Range Dependence and Sea Level Forecasting*; Springer: Berlin/Heidelberg, Germany, 2013.
91. Barbosa, S.; Fernandes, M.; Silva, M. Long-range dependence in North Atlantic sea level. *Physica A* **2006**, *371*, 725–731.
92. Beretta, A.; Roman, H.E.; Raicich, F.; Crisciani, F. Long-time correlations of sea-level and local atmospheric pressure fluctuations at Trieste. *Physica A* **2005**, *347*, 695–703.
93. Li, M.; Cattani, C.; Chen, S.Y. Viewing sea level by a one-dimensional random function with long memory. *Math. Probl. Eng.* **2011**, *2011*, doi:10.1155/2011/654284.
94. Beran, J. Statistical methods for data with long-range dependence. *Stat. Sci.* **1992**, *7*, 404–416.
95. Jiao, Z.; Chen, Y.-Q.; Podlubny, I. *Distributed-Order Dynamic Systems*; Springer: Berlin/Heidelberg, Germany, 2011.
96. Sheng, H.; Chen, Y.-Q.; Qiu, T.-S. *Fractional Processes and Fractional Order Signal Processing*; Springer: Berlin/Heidelberg, Germany, 2012.

97. Sun, H.G.; Chen, Y.-Q.; Chen, W. Random-order fractional differential equation models. *Signal Process.* **2011**, *91*, 525–530.
98. Muniandy, S.V.; Chew, W.X.; Wong, C.S. Fractional dynamics in the light scattering intensity fluctuation in dusty plasma. *Phys. Plasmas* **2011**, *18*, 013701.
99. Asgari, H.; Muniandy, S.V.; Wong, C.S. Stochastic dynamics of charge fluctuations in dusty plasma: A non-Markovian approach. *Phys. Plasmas* **2011**, *18*, 083709.
100. Eab, C.H.; Lim, S.C. Accelerating and retarding anomalous diffusion. *J. Phys. A* **2012**, *45*, 145001.
101. Yang, X.-J.; Srivastava, H.M.; He, J.-H.; Baleanu, D. Cantor-type cylindrical-coordinate method for differential equations with local fractional derivatives. *Phys. Lett. A* **2013**, *377*, 1696–1700.
102. Yang, X.-J.; Baleanu, D. Fractal heat conduction problem solved by local fractional variation iteration method. *Therm. Sci.* **2013**, *17*, 625–628.
103. Cattani, C.; Ciancio, A. Separable transition density in the hybrid model for tumor-immune system competition. *Comput. Math. Methods Med.* **2012**, *2012*, 610124.
104. Cattani, C.; Ciancio, A.; Lods, B. On a mathematical model of immune competition. *Appl. Math. Lett.* **2006**, *19*, 678–683.
105. Bakhoum, E.G.; Toma, C. Mathematical transform of traveling-wave equations and phase aspects of quantum interaction. *Math. Probl. Eng.* **2010**, *2010*, doi:10.1155/2010/695208.
106. Toma, C. Advanced signal processing and command synthesis for memory-limited complex systems. *Math. Probl. Eng.* **2012**, *2012*, doi: 10.1155/2012/927821.
107. Beran, J.; Shernan, R.; Taqqu, M.S.; Willinger, W. Long-range dependence in variable bit-rate video traffic. *IEEE Trans. Commun*. **1995**, *43*, 1566–1579.
108. Gu, C.G.; Coomans, C.P.; Hu, K.; Scheer, F.A.J.L.; Stanley, H.E.; Meijer, J.H. Lack of exercise leads to significant and reversible loss of scale invariance in both aged and young mice. *Proc. Natl. Acad. Sci. USA* **2015**, *112*, 2320–2324.
109. Lévy Véhel, J. Beyond multifractional Brownian motion: New stochastic models for geophysical modeling. *Nonlinear Process. Geophys.* **2013**, *20*, 643–655.
110. Pinchas, M. Symbol error rate for non-blind adaptive equalizers applicable for the SIMO and FGn case. *Math. Probl. Eng.* **2014**, *2014*, doi:10.1155/2014/606843.
111. Arzano, M.; Calcagni, G. Black-hole entropy and minimal diffusion. *Phys. Rev. D* **2013**, *88*, 084017.
112. Werner, G. Fractals in the nervous system: conceptual implications for theoretical neuroscience. *Front. Physiol.* **2010**, *1*, doi:10.3389/fphys.2010.00015.
113. Zhao, S.X.; Ye, F.Y. Power-law link strength distribution in paper cocitation networks. *J. Am. Soc. Inf. Sci. Technol.* **2013**, *64*, 1480–1489.
114. Kaklauskas, L.; Sakalauskas, L. Study of on-line measurement of traffic self-similarity. *Cent. Eur. J. Oper. Res.* **2013**, *21*, 63–84.
115. Chen, C.-C.; Lee, Y.-T.; Hasumi, T.; Hsu, H.-L. Transition on the relationship between fractal dimension and Hurst exponent in the long-range connective sandpile models. *Phys. Lett. A* **2011**, *375*, 324–328.
116. Wang, X.J.; Shang, P.J.; Fang, J.T. Traffic time series analysis by using multiscale time irreversibility and entropy. *Chaos* **2014**, *24*, 032102.

117. Reyes, J.; Morales-Esteban, A.; Martinez-Alvarez, F. Neural networks to predict earthquakes in Chile. *Appl. Soft Comput.* **2013**, *13*, 1314–1328.
118. Lee, J.S.R.; Ye, S.K.; Jeong, H.D.J. ATMSim: An anomaly teletraffic detection measurement analysis simulator. *Simul. Model. Pract. Theory* **2014**, *49*, 98–109.
119. Wang, D.M.; Li, Y.; Nie, P.F. A Study on the Gaussianity and Stationarity of the Random Noise in the Seismic Exploration. *J. Appl. Geophys.* **2014**, *109*, 210–217.
120. Ye, X.; Xia, X.; Zhang, J.; Chen, Y. Effects of trends and seasonalities on robustness of the Hurst parameter estimators. *IET Signal Process.* **2012**, *6*, 849–856.
121. Ghizdavet, Z.; Gradinaru, R. Heat balance computation on a clinkering plant over different time steps. *Revista Romana De Materiale* **2013**, *43*, 332–338.
122. Uritsky, V.M.; Slavin, J.A.; Khazanov, G.V.; Donovan, E.F.; Boardsen, S.A.; Anderson, B.J.; Korth, H. Kinetic-scale magnetic turbulence and finite Larmor radius effects at Mercury. *J. Geophys. Res. Space Phys.* **2011**, *116*, doi:10.1029/2011JA016744.
123. Ghasemi, F.; van Ommen, J.R.; Sahimi, M. Analysis of pressure fluctuations in fluidized beds. I, Similarities with turbulent flow. *Chem. Eng. Sci.* **2011**, *66*, 2627–2636.
124. Schaefer, A.; Brach, J.S.; Perera, S.; Sejdic, E. A comparative analysis of spectral exponent estimation techniques for $1/f^{\beta}$ processes with applications to the analysis of stride interval time series. *J. Neurosci. Methods* **2014**, *222*, 118–130.
125. Mandelbrot, B.B. *Gaussian Self-Affinity and Fractals*; Springer: Berlin, Germany, 2001.